MIT Open Access Articles

Sensitivity comparison of searches for binary black hole coalescences with ground-based gravitational-wave detectors

Sensitivity comparison of searches for binary black hole coalescences with ground-based gravitational-wave detectors

Satya Mohapatra,[1,2,3] Laura Cadonati,[1,4] Sarah Caudill,[5,6] James Clark,[1] Chad Hanna,[7] Sergey Klimenko,[8]
Chris Pankow,[5] Ruslan Vaulin,[9] Gabriele Vedovato,[10] and Salvatore Vitale[9]

[1]*University of Massachusetts–Amherst, Amherst, Massachusetts 01003, USA*
[2]*Rochester Institute of Technology, 85 Lomb Memorial Drive, Rochester, New York 14623, USA*
[3]*Syracuse University, Syracuse, New York 13244, USA*
[4]*Cardiff University, Cardiff CF24 3AA, United Kingdom*
[5]*University of Wisconsin–Milwaukee, Milwaukee, Wisconsin 53201, USA*
[6]*Louisiana State University, Baton Rouge, Louisiana 70803, USA*
[7]*Pennsylvania State University, University Park, Pennsylvania 16802, USA*
[8]*University of Florida, Gainesville, Florida 32611, USA*
[9]*LIGO, Massachusetts Institute of Technology, Cambridge, Massachusetts 02139, USA*
[10]*INFN Sezione di Padova, 35131 Padova, Italy*

Searches for gravitational-wave transients from binary black hole coalescences typically rely on one of two approaches: matched filtering with templates and morphology-independent excess power searches. Multiple algorithmic implementations in the analysis of data from the first generation of ground-based gravitational-wave interferometers have used different strategies for the suppression of non-Gaussian noise transients and have targeted different regions of the binary black hole parameter space. In this paper we compare the sensitivity of three such algorithms: matched filtering with full coalescence templates, matched filtering with ringdown templates, and a morphology-independent excess power search. The comparison is performed at a fixed false alarm rate and relies on Monte Carlo simulations of binary black hole coalescences for spinning, nonprecessing systems with a total mass of 25–350 $M_\odot$, which covers a portion of the parameter space of stellar mass and intermediate mass black hole binaries. We find that in the mass range of 25–100 $M_\odot$, the sensitive distance of the search, marginalized over source parameters, is the best with matched filtering to full waveform templates, which is within 10% of the next most sensitive search of morphology-independent excess power algorithm, at a false alarm rate of 3 events/year. In the mass range of 100–350 $M_\odot$, the same comparison favors the morphology-independent excess power search within 20% of matched filtering with ringdown templates. The dependence on mass and spin is also explored.

I. INTRODUCTION

Binary black hole coalescences are amongst the most promising sources of gravitational-wave transients for ground-based gravitational-wave observatories such as Laser Interferometer Gravitational-wave Observatory (LIGO) and Virgo [1–3]. While stellar mass black holes with mass between 2.5 $M_\odot$ and a few tens of $M_\odot$ are formed by stellar collapse [4–7], intermediate mass black holes between a few tens of $M_\odot$ and 10^5 $M_\odot$ may result from the merger of stellar mass black holes or runaway collision of massive stars in dense globular clusters [8–10]. No evidence of binary black hole coalescence has been detected so far in data from initial LIGO and Virgo [11–17]. However, according to current rate predictions, advanced LIGO [18] and advanced Virgo [19] are expected to detect several gravitational-wave signals from binary black hole coalescences [20].

Following the seminal work of [21], LIGO and Virgo data have been searched for separate phases of the binary black hole coalescence: inspiral, merger, and ringdown [11,12,16,22]. Search methods have evolved to account for full inspiral-merger-ringdown waveform templates [13], use signal based vetoes [23], employ multiresolution time-frequency information [24], and utilize coincident and coherent methods [22,25,26].

This paper compares different searches in real detector noise and applies it to algorithms representative of those used in recent searches for binary black holes in LIGO and Virgo data [13–15,17,22,26]. Section II describes the data used in this study. Section III introduces the search algorithms that are compared in this study. Section IV outlines the method used in the comparison, and Sec. V presents the results, using three complementary figures of merit: efficiency curve in Fig. 4, mean sensitive distance in Fig. 5, and sensitive distance in Figs. 6, 7, 10, and 11.

II. DETECTOR DATA

We conducted this study on a two-months subset (14 August to 30 September 2007) of data from the fifth
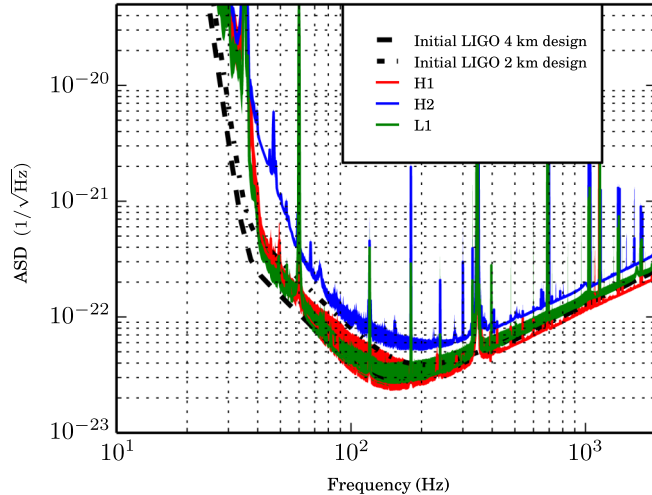
FIG. 1 (color online). Sensitivity of the detectors during the period of data in this study. The color shaded region indicates the 5th to 95th amplitude spectral density percentiles.

science run LIGO, when initial LIGO was at design sensitivity [27]. We considered the three-detector network of the 4-km and 2-km Hanford (H1, H2) [28], and 4-km Livingston (L1) [29] observatories. Figure 1 shows the detectors' sensitivity, expressed as strain amplitude spectral density (ASD). The color shaded region indicates the 5th to 95th ASD percentiles in the analyzed period.

Data below 40 Hz is not included in this analysis since it is limited by the seismic noise and, therefore, is not calibrated [30]. We applied data selections and vetoes to account for environmental artifacts and instrumental glitches that affect the quality and reliability of the data; this, combined with the instruments' duty cycle, resulted in a 3-detector lifetime of 29 days. See [31,32] for details of this procedure.

III. SEARCH ALGORITHMS

Transient gravitational-wave searches can be broadly classified into matched filtering with templates and unmodeled searches which do not assume a specific signal model. Matched filtering can be performed with templates for the full binary black hole coalescence or only a portion of it. Unmodeled searches look for statistically significant excess signal energy in gravitational-wave data. In this paper we consider three algorithms that have been adopted in searches of LIGO-Virgo data: the inspiral-merger-ringdown (IMR)-templates search [13,14], the ringdown search [15,22], and Coherent WaveBurst [16,17].

A. IMR templates

Matched filtering to a bank of nonspinning Effective One Body tuned to Numerical Relativity templates [33] has been used to search for binary black hole mergers in 25–100 $M_\odot$ [13,14]. Matched filtering is optimal for weak signals in Gaussian noise. However, due to the

nonstationary, non-Gaussian nature of LIGO-Virgo data, this search is augmented with a sophisticated intersite coincidence test [25], a time-frequency, χ^2 signal consistency test [23], and a combined false alarm rate event ranking, all of which are described in Sec. 3 of [13].

B. Ringdown search

The postmerger signal is accurately described as a superposition of quasinormal oscillation modes, the *ringdown* waveforms [34]. Searches for ringdowns utilize a matched filtering algorithm with damped sinusoidal templates characterized by quality factor Q and central frequency f_0, parameters that describe the $\ell = m = 2$ oscillation mode of the final merged black hole [15,22,35]. Details on the template bank and the algorithm are given in [15]. The central frequency and quality factor can be empirically related to the final mass and spin of the merged black hole [36]; the search space corresponds roughly to black holes with masses in the range 10 $M_\odot$ to 600 $M_\odot$ and spins in the range 0 to 0.99.

The ringdown matched filter search is also augmented with a sophisticated multidetector coincidence test [25,37], an amplitude consistency test [15], and an event ranking based on the *chopped-L statistic* described in [38]. This event ranking statistic differs from the multivariate statistic used in [15]. Candidate events are ranked with the combined false alarm rate detection statistic described in [13,15].

C. Coherent WaveBurst

The Coherent WaveBurst (CWB) algorithm is designed to identify coherent excess power transients without prior knowledge of the waveform, and it is used in searches for gravitational-wave bursts in LIGO and Virgo data [32,39]. By imposing weak model constraints, such as the requirement of elliptical polarization, CWB has been optimized to search for black hole binaries of total masses between 100 and 450 $M_\odot$ [16,17].

The algorithm uses a wavelet basis to decompose the data into a time-frequency map with discrete signal energy pixels. The algorithm then executes a constrained maximum likelihood analysis of the decomposed network data stream. Reconstruction of detector responses occurs for a trial set of sky locations and corresponding arrival delays. The residual data, after subtraction of the estimated detector responses from the original data, represents the reconstructed network noise. The elliptical polarization constraint is expected to have minimal impact on the recovery of gravitational-wave signals from compact binary coalescences while enhancing the rejection of noisy events [40].

The coherent network amplitude η is the detection statistic used by CWB [16,17]. It is proportional to the average signal-to-noise ratio (SNR) per detector and is used to rank selected events and establish their significance against a sample of background events.

IV. COMPARISON METHOD

Since the algorithms described in Sec. III have different targets, it is natural to expect they respond differently to weak signals in the data and to noise transients. In this paper we compare the sensitivity of the three searches by evaluating the efficiency with which injected signals can be detected at a given false alarm rate, which ranks an event's rate of occurrence, as determined from a background sample. We ran the analyses with configurations that are representative of their applications in published results [13–17,22].

For this analysis, we injected simulated gravitational-wave signals from the coalescence of binary black holes into initial LIGO strain data. The waveforms were produced with the IMRPhenomB [41] model: a phenomenological, nonprecessing, spinning binary black hole template family which tracks the coalescence from late inspiral to ringdown. In this configuration, the spin vectors (χ_1 and χ_2) are aligned/antialigned with the angular momentum of the binary system. The waveforms are parametrized by three physical parameters: the component black hole masses m_1 and m_2 and the mass weighted spin parameter χ_s,

$$\chi_s = \frac{m_1\chi_1 + m_2\chi_2}{m_1 + m_2}. \qquad (1)$$

The waveforms do not include the effects of nonaligned spin-orbit coupling but do account for aligned/antialigned spin-orbit interaction, such as the orbital hang-up effect [42].

To determine the false alarm rate, we time shifted the data from one or more detectors well beyond the light travel time of 10 ms between H1 and L1. We imposed a minimum shift of 5 seconds to remove intersite correlations which could be due to a real gravitational-wave signal in the data. We did not introduce time shifts between data from the colocated H1 and H2 detectors since the background noise from these detectors was correlated [13]. We applied 100 equally spaced time shifts in the ringdown and the IMR-template searches, and 600 in the CWB search. We declared an injection *detected* if a coincident event was identified within 100 ms of the nominal injection time. This interval is long enough to account for the uncertainty in identifying the *arrival time* of a signal, where the arrival time is the maximum amplitude of the waveform.

Each pipeline ranked all of the events and assigned a false alarm rate by comparison with respective background ranking statistics. We evaluated detection efficiency and sensitive distance (as defined in Sec. V) for a range of measurable false alarm rate thresholds. We quote the results for a false alarm rate threshold of 3 events per year, which is in the middle of this range. We made sure that the searches use consistent data after the application of data quality vetoes, with small differences due to technical details in the veto implementation [31].

V. RESULTS

A. Target parameter space

In this study, we partitioned the parameter space according to the total mass of the binary system. *Set A* includes systems with total mass between 25 and 100 $M_\odot$, as searched by IMR templates [13,14]. *Set B* consists of total mass between 100 and 350 $M_\odot$, which overlaps the parameter space searched by the CWB algorithm [16,17]. We restricted the total mass to below 350 $M_\odot$ as the peak detectable frequencies from the ringdown, for some of the spin configuration is below 40 Hz for mass above 350 $M_\odot$ [41,43] and thus is subject to unacceptable or ill-defined uncertainties arising from calibration [30].

Simulated signals are uniformly distributed in total mass (m), mass ratio (q), and dimensionless spin parameter χ_s, in the intervals listed in Table I. This distribution is not meant to reproduce the expected astrophysical distribution of binary black hole sources, but rather to probe a wide physical parameter space and evaluate the efficacy of each pipeline in detection. The injections are logarithmically distributed in distance. No correction to the waveform due to redshift at cosmological distances is included, as this effect is expected to be small ($z <= 0.1$) at the reach of initial detectors. Injections are also uniformly distributed in sky location, polarization, and inclination of the binary relative to Earth.

We analyzed ~25000 injections; due to the limitations of the search (i.e., reduced efficacy of χ^2 above 100 $M_\odot$, as discussed in Sec. III), we used the IMR-templates search only for the lower mass set of injections. We performed ringdown matched filter and CWB analyses on both injection sets.

Before discussing the results evaluated for the three search algorithms, we show the *expected range* as a function of total mass, mass ratio, and spin parameter in Figs. 2 and 3. The expected range is calculated by averaging the distances over extrinsic parameters such as sky position and inclination of the binary black holes for which the network SNR is 12, following the prescription used in [44]. The SNR is estimated from the median value of the amplitude spectral density of the instrumental noise in Fig. 1. Expected distance gives a search-algorithm independent, theoretical measure of sensitivity which is later compared with the sensitivity obtained from the three search algorithms.

Figure 2 illustrates that the expected range is higher for symmetric mass binary black holes compared to asymmetric mass system for the same total mass. This is

TABLE I. Simulated waveform parameters.

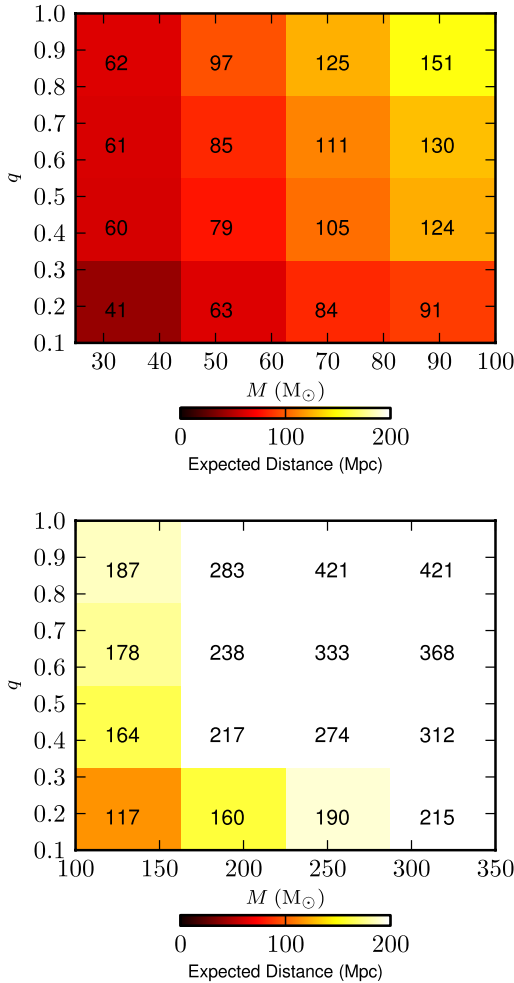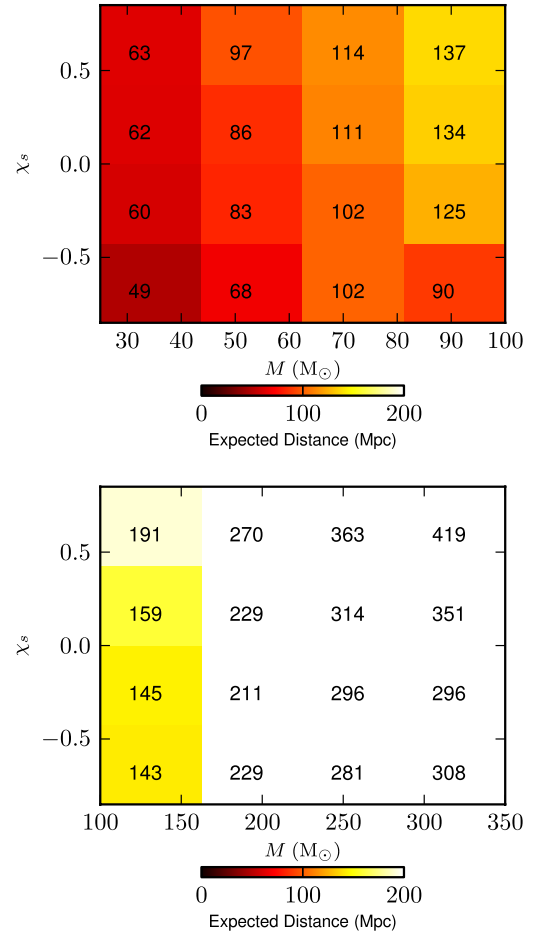|	
Total Mass ($M_\odot$), m: Set A	25–100
Total Mass ($M_\odot$), m: Set B	100–350
Mass Ratio (both sets), q:	0.1–1
χ_s (both sets)	−0.85–0.85
Distance (Mpc) (both sets)	0–2000

FIG. 2 (color online).   Expected range (Mpc) as a function of *m* vs *q*. This quantity is estimated from the network SNR threshold of 12 and is marginalized over the spin parameter, sky position, and orientation of the binary system. The color scale is saturated at 200 Mpc for comparison with Figs. 6, 7, 10, and 11.

FIG. 3 (color online).   Expected range (Mpc) as a function of *m* vs χ_s. This quantity is estimated at a network SNR threshold of 12 and is marginalized over mass ratio, sky position, and orientation of the black hole binary system.

consistent with the fact that the SNR of the signal is proportional to its amplitude divided by the square root of its duration in time. For a binary black hole, the gravitational-wave amplitude is proportional to $\frac{q}{(1+q)^2}$, while the time duration is proportional to $\frac{(1+q)^2}{q}$; hence SNR is proportional to $\frac{\sqrt{q}}{1+q}$ [45]. Figure 3 illustrates that the expected range is higher for aligned than for antialigned spin configurations since systems with aligned spins stay longer in orbit until merger—hence get more relativistic, leading to higher gravitational-wave luminosity—than anti-aligned systems [42].

B. Search performance

We now define the quantities that will be used for the comparison. The detection efficiency ε of a search is a function of the false alarm rate threshold ζ, the radial distance to the source r, the total mass m, the mass ratio q, and the spin parameter χ_s. In this work, we average over sky location, polarization, and orientation and define the average efficiency as

$$\bar{\varepsilon}(\zeta, r, m, q, \chi_s) = \frac{N_f}{N_i}, \qquad (2)$$

where N_f is the number of found injections and N_i is the number of total injections averaged over all sky position and inclination.

The sensitive volume, or the volume of the sky surveyed, is defined as

$$V(\zeta, m, q, \chi_s) = \int 4\pi r^2 \bar{\varepsilon}\, dr. \qquad (3)$$

Finally, the sensitive radius $\mathcal{R}$ is the radius of the sphere with volume of V:
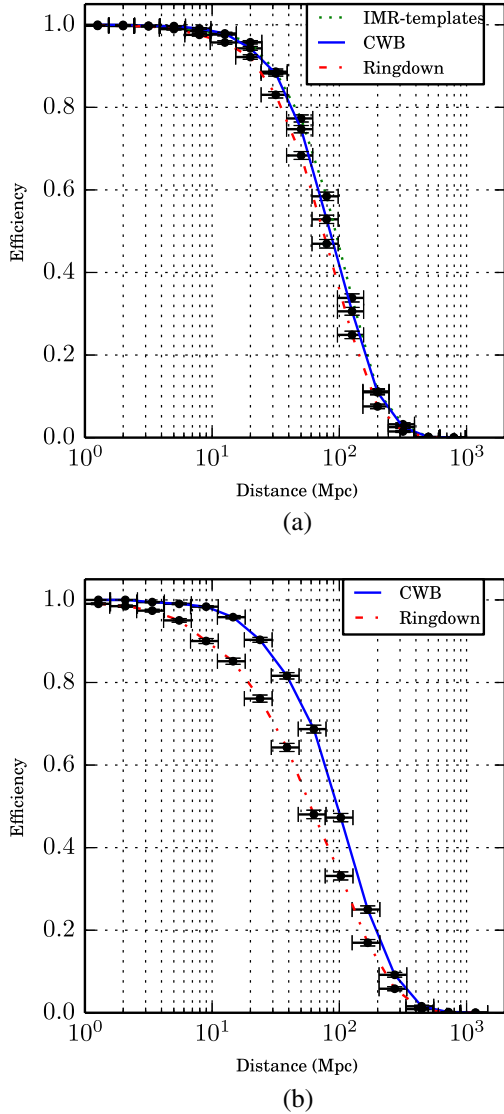
(a)

(b)

FIG. 4 (color online).   Efficiency curves at a false alarm rate of 3 events per year, averaged over total mass, mass ratio, spin parameter, sky position, and inclination of the source. (a) Total mass 25–100 $M_\odot$. (b) Total mass 100–350 $M_\odot$.

$$\mathcal{R}(\zeta, m, q, \chi_s) = \left[\frac{3}{4\pi}V\right]^{1/3}. \qquad (4)$$

1. Efficiency curves

The detection efficiency at fixed false alarm rate and distance is estimated from Eq. (2); we plot it as a function of distance in Fig. 4, where N_i and N_f are marginalized over all other source parameters. The horizontal and the vertical error bars in Fig. 4 are set by the bin boundaries and binomial statistics on the number of injected signals in each amplitude bin, respectively.

For a quantitative comparison, we fit a cubic spline to the efficiency curve. We then compare two characteristic parameters, the 50% and 90% efficiency distances, $D_{eff}^{50\%}$

TABLE II.   Efficiency distances at a false alarm rate of 3 events per year.

Algorithm (on Set A)	$D_{eff}^{50\%}$ (Mpc)	$D_{eff}^{90\%}$ (Mpc)
IMR-templates search	94	30
CWB	84	28
Ringdown	75	23
Algorithm (on Set B)	$D_{eff}^{50\%}$ (Mpc)	$D_{eff}^{90\%}$ (Mpc)
CWB	97	24
Ringdown	60	9

and $D_{eff}^{90\%}$, which are the distances at which 50% and 90% of the signals can be found, respectively, in Table II.

In the 25–100 $M_\odot$ range (Set A), the IMR templates search yields 12% and 25% higher $D_{eff}^{50\%}$ and 7% and 30%
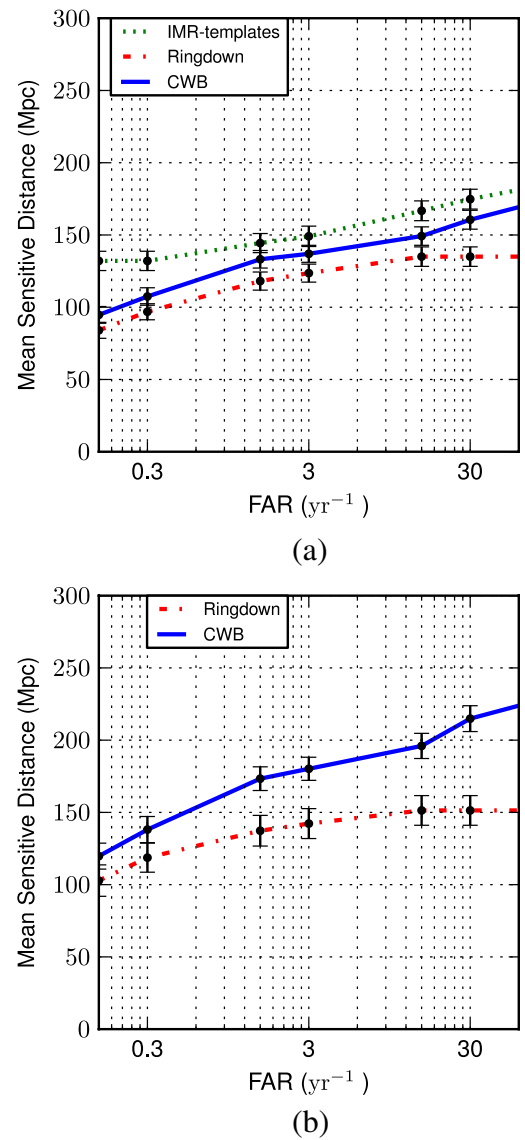

(a)

(b)

FIG. 5 (color online).   Mean sensitive distance as a function of false alarm rate. (a) Total mass 25–100 $M_\odot$. (b) Total mass 100–350 $M_\odot$.
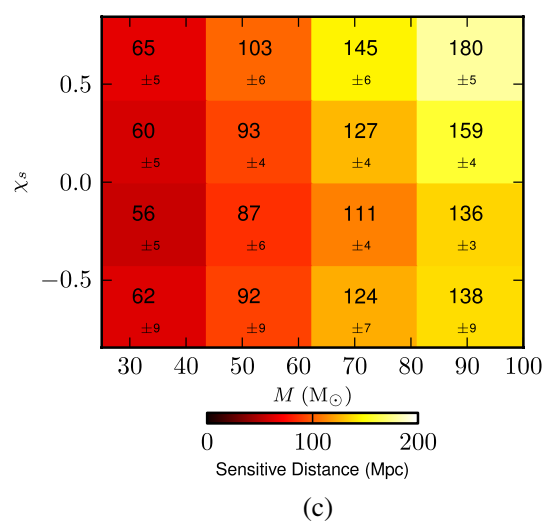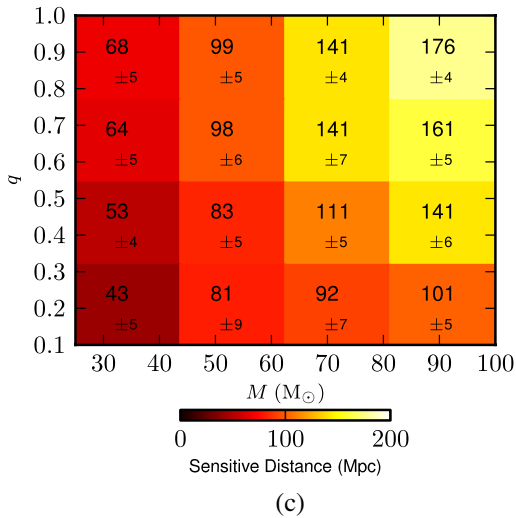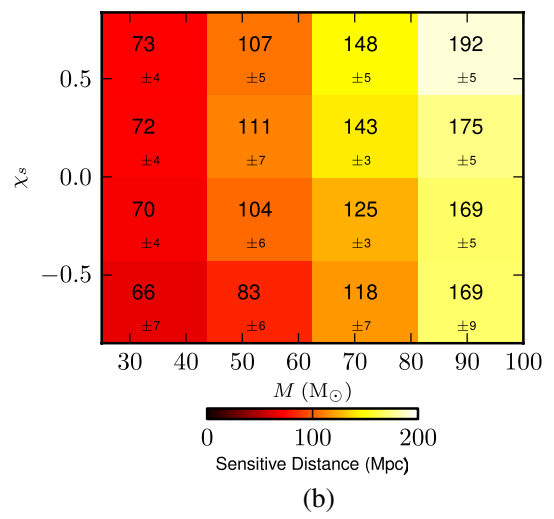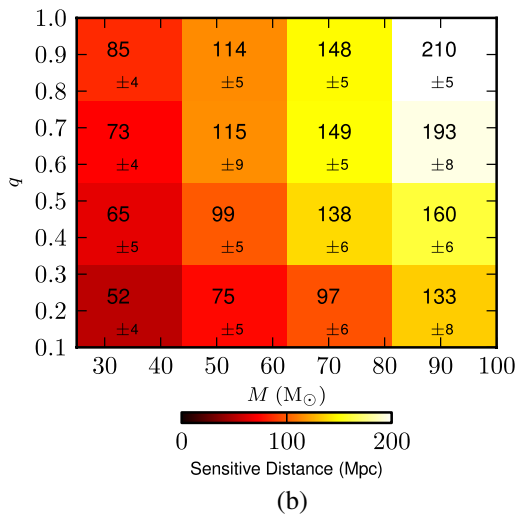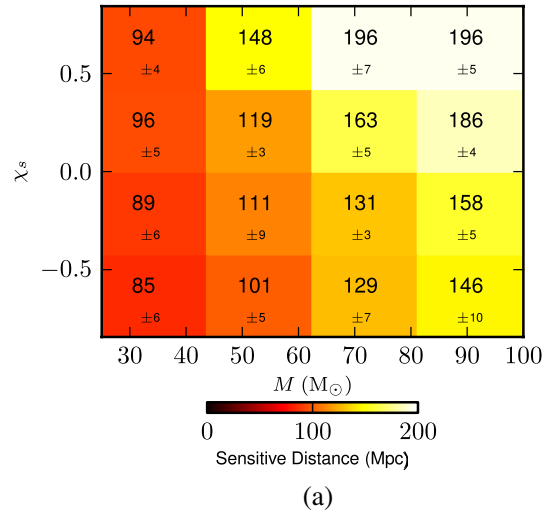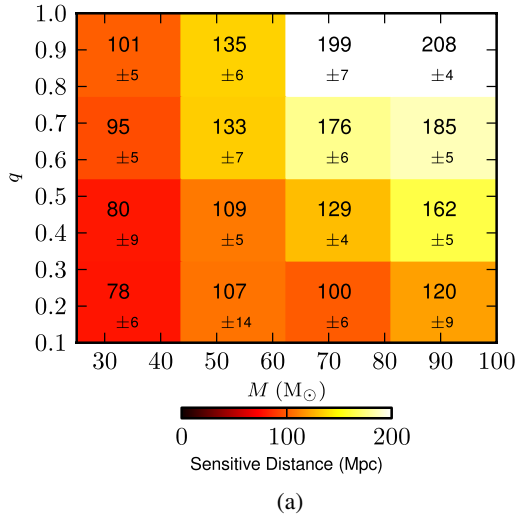
FIG. 6 (color online). Sensitive distance for systems with total mass 25–100 $M_\odot$ as a function of total mass m and mass ratio q at a false alarm rate of 3 events per year. (a) Matched filter to IMR templates. (b) Coherent WaveBurst template-less search. (c) Matched filter to ringdowns.

FIG. 7 (color online). Sensitive distance for systems with total mass 25–100 $M_\odot$ as a function of total mass m and mass ratio χ_s at a false alarm rate of 3 events per year. (a) Matched filter to IMR templates. (b) Coherent WaveBurst template-less search. (c) Matched filter to ringdowns.

higher $D_{\text{eff}}^{90\%}$ compared to the CWB and the ringdown searches, respectively. In the 100–350 $M_\odot$ range (Set B), the CWB search yielded 60% higher $D_{\text{eff}}^{50\%}$ and 170% higher $D_{\text{eff}}^{90\%}$ compared to the ringdown search.

2. Mean sensitive distance

Equation (4) can be marginalized over all parameters to compute a mean sensitive distance as a function of the false alarm rate. This quantity is shown in Fig. 5.

We notice that within a range of false alarm rates of 0.3 events per year to 30 events per year, the three searches give consistent results. We do not see any abrupt change of sensitivity for a search over this range of false alarm rates. The false alarm rate of 3 events/year we chose to plot efficiency curves and quote sensitive

distances is thus representative of the relative performance of the algorithms.

Published searches have typically chosen lower false alarm rate thresholds estimated on the loudest events [46,47] seen by the searches in open-box data: 0.2 events/year and 0.41 events/year for IMR-template searches on 2005–2007 [13] and 2009–2010 [14] LIGO-Virgo data, 0.45 events/year for the ringdown search [15], and 0.76 events/year for the CWB search on 2005–2007 data [16].

3. Sensitive distance

To probe how different algorithms respond to different regions of the parameter space, we plot the sensitive distance, defined in Eq. (4), as a function of the mass and spin parameters at a false alarm rate of 3 events per year. Additional sensitive distance plots in between 0.3 to 30 events per year are available at [48].
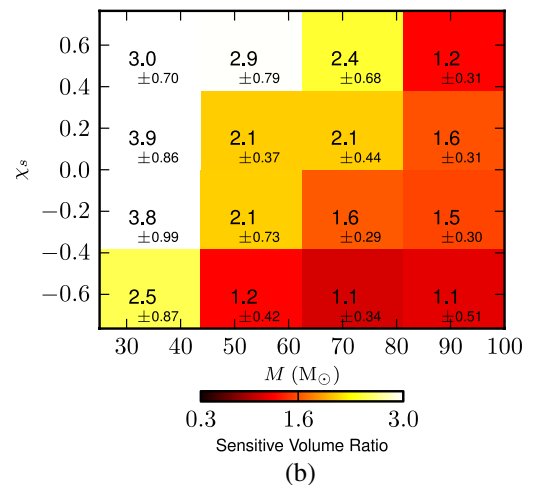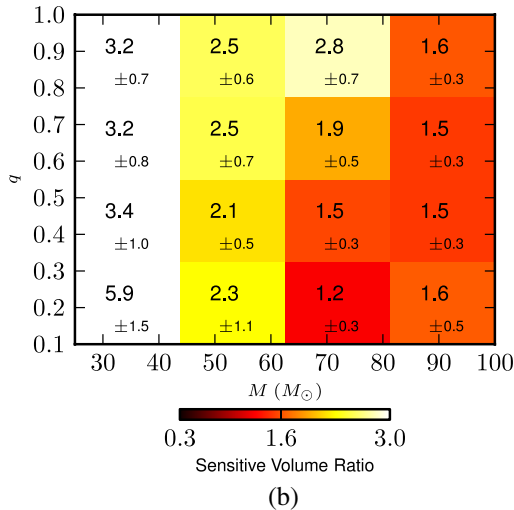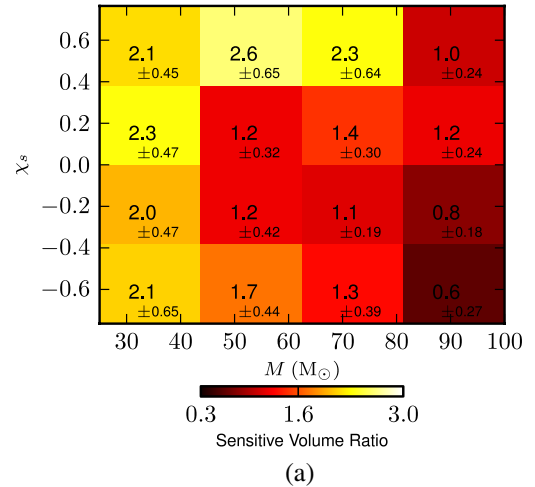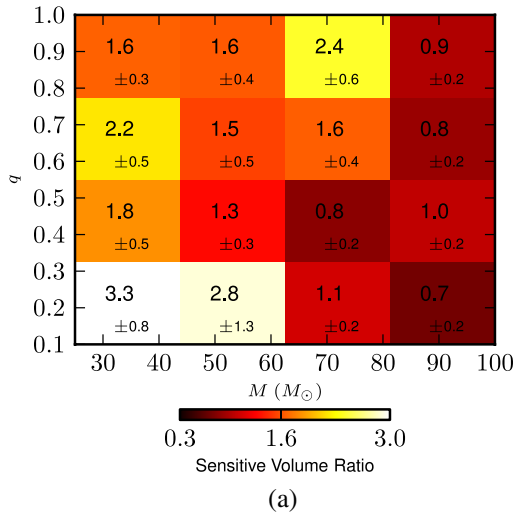

(a)

(b)

FIG. 8 (color online).   Sensitive volume ratio for systems with total mass 25–100 $M_\odot$ as a function of m and q at a false alarm rate of 3 events per year. (a) IMR templates/Coherent WaveBurst. (b) IMR templates/ringdown.

(a)

(b)

FIG. 9 (color online).   Sensitive volume ratio for systems with total mass 25–100 $M_\odot$ as a function of m vs χ_s at a false alarm rate of 3 events per year. (a) IMR templates/Coherent WaveBurst. (b) IMR templates/ringdown.

Figures 6 and 10 show the sensitive distance at false alarm rate threshold of 3 events per year as a function of mass parameters m and q and are marginalized over the spin parameter χ_s. Across the mass ranges, the three search algorithms are more sensitive to symmetric than asymmetric binary systems.

For Set A all three search algorithms have the highest sensitive distance in the total mass bin of 80 to 100 $M_\odot$. For Set B the CWB search and the ringdown search register higher sensitive distance in the total mass bin of 100 to 150 $M_\odot$.

Figures 7 and 11 show the sensitive distance as a function of total mass and the spin parameter and are marginalized over mass ratio q. Across the mass ranges, the three search algorithms have higher sensitivity for detecting aligned (with respect to the orbital angular momentum)

spin binary black holes compared to the antialigned spin binary black holes [14,17,49]. Qualitatively, this observation is consistent with the expected range in Fig. 3. Quantitatively, sensitive distance differs from the expected range, which motivates the choice of false alarm rate as the criteria for detectability, rather than the signal SNR.

The errors quoted in Figs. 6, 7, 10, and 11 are derived from the binomial statistics of events in each bin.

Figure 8 shows the ratio in the sensitive volume, defined in Eq. (3), for Set A injections in total mass and mass ratio, and Fig. 9 shows that ratio for total mass and spin parameter space. In these plots the significance, i.e., σ deviation, of the sensitive volume ratio with respect to the associated errors is shown in each bin. For this set the IMR-template search shows higher sensitivity compared to the ringdown search and the CWB search across the parameter space. The higher sensitivity of the IMR-template search is significantly more with
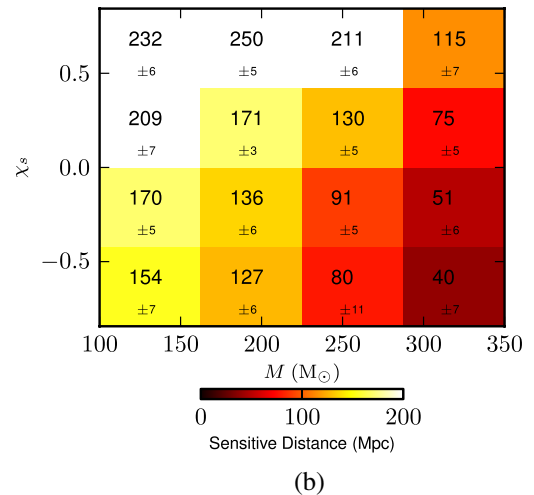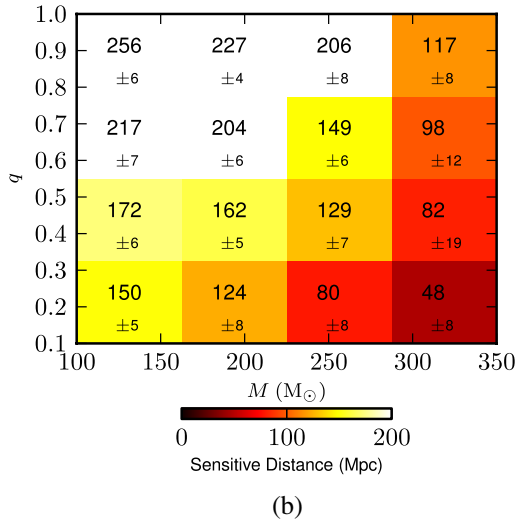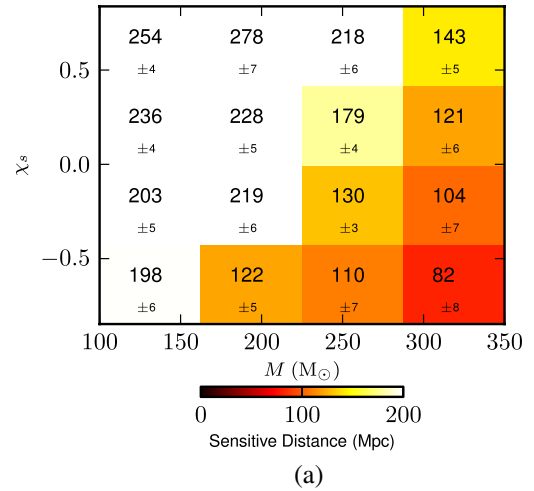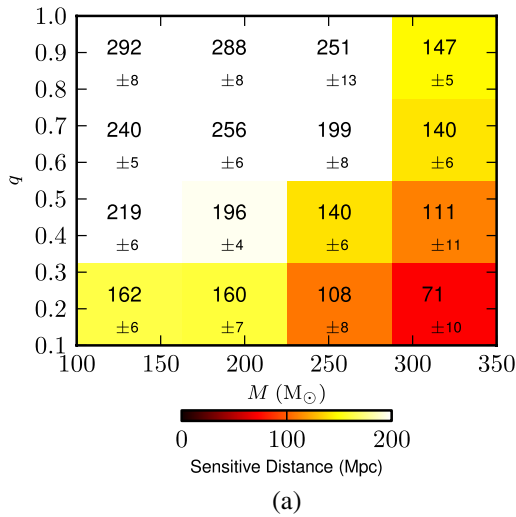

FIG. 10 (color online).   Sensitive distance for systems with total mass 100–350 $M_\odot$ as a function of m and q at a false alarm rate of 3 events per year. (a) Coherent WaveBurst template-less search. (b) Matched filter to ringdowns.

FIG. 11 (color online).   Sensitive distance for systems with total mass 100–350 $M_\odot$ as a function of m and χ_s at a false alarm rate of 3 events per year. (a) Coherent WaveBurst template-less search. (b) Matched filter to ringdowns.
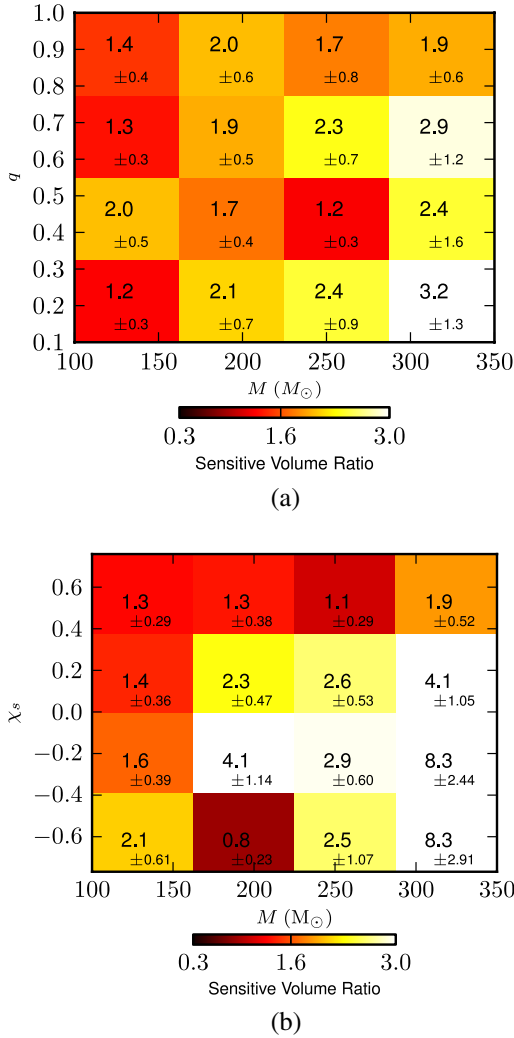
FIG. 12 (color online). Sensitive volume ratio for systems with total mass 100–350 $M_\odot$ as a function of m and q, and m and χ_s at a false alarm rate of 3 events per year. (a) Coherent WaveBurst/ringdown. (b) Coherent WaveBurst/ringdown.

respect to the ringdown search in comparison with the CWB search. The significance is higher for binary black holes with spin aligned to the angular momentum. The CWB search has more sensitivity compared to the ringdown search for this mass range, albeit within 2σ deviation only.

Figure 12 shows the ratio of the sensitive volume for Set B injections in total mass, mass ratio, and total mass spin parameter space. Across the parameter space, CWB is more sensitive than the ringdown search, albeit with varying degrees of significance.

VI. CONCLUSION

This paper compares searches for binary black hole coalescences in ground-based gravitational-wave detectors and applies it to algorithms used in recently published

searches [13–17] on a two-month segment of initial LIGO data. The codes developed for this analysis are available in the LIGO Scientific Collaboration Algorithm Library software packages [50].

This is the first one-on-one comparison of searches for binary black hole coalescences. The false alarm rate of 3 events per year is a prefatory choice for the demonstration of the method. This analysis provides the groundwork for future work, which will include a comparison of algorithms at detection-level false alarm rate and which requires significant computational resources.

We provide a quantitative measure of how the algorithms tested in this study were more sensitive to symmetric than asymmetric systems, and to aligned rather than antialigned binary black holes. Additionally, we probe the different sensitivity of the algorithms to different regions of the black hole binary parameter space. We find that a matched filtering search algorithm using the full inspiral-merger-ringdown templates is the most sensitive search algorithm for total mass between 25 and 100 $M_\odot$: 6% more than a morphology-independent excess power search and 17% more than matched filtering to ringdown templates, by the measurement of sensitive distance averaged over source parameters at a false alarm rate of 3 events/year. A fully coherent gravitational-wave burst search algorithm is 21% more sensitive compared to the matched filtering search algorithm with ringdown templates, by the measurement of sensitive distance averaged over source parameters at a false alarm rate of 3 events/year.

This was a nonblind analysis, as the characteristics of simulated signals were known *a priori*. The ability to detect binary black hole coalescence signals through different search algorithms in a blind analysis has been shown in a different study [49]. Also, this work does not attempt to combine information from searches. A likelihood based method to combine multiple searches has been prescribed in [51].

In this study we have relied on nonprecessing phenomenological waveform model. As new template families with wider coverage of the parameter space are now becoming available [52–54], the method prescribed in this paper can readily be extended to them. We also note that the analysis presented in this paper relies on the initial LIGO sensitivity. We expect differences will ensue with the different possible noise spectra expected in advanced LIGO [55–57] and advanced Virgo [58]. Additionally, we do not expect the population of non-Gaussian noise transients to be the same in advanced LIGO/Virgo as in initial LIGO/Virgo data. New algorithms and pipeline improvements are currently under development; for instance, the inclusion of spinning templates in the bank for IMR templates [59], different clustering in the CWB search, and a more sophisticated postprocessing for the ringdown search [15]; the relative performance of the searches may need to be reassessed once such developments have stabilized.

ACKNOWLEDGMENTS

[1] *300 Years of Gravitation*, edited by S. Hawking and W. Israel (Cambridge University Press, Cambridge, England, 1987).

[2] B. P. Abbott *et al.* (LIGO Scientific Collaboration), Rep. Prog. Phys. **72**, 076901 (2009).

[3] F. Acernese *et al.* (Virgo Collaboration), J. Opt. A **10**, 064009 (2008).

[4] S. L. Shapiro and S. A. Teukolsky, *Black Holes, White Dwarfs and Neutron Stars: The Physics of Compact Objects* (John Wiley & Sons, New York, 1983).

[5] T. Bulik, K. Belczynski, and A. Prestwich, Astrophys. J. **730**, 140 (2011).

[6] K. Belczynski, M. Dominik, T. Bulik, R. O, Shaughnessy, C. Fryer, and D. E. Holz, Astrophys. J. Lett. **715**, L138 (2010).

[7] M. Dominik, K. Belczynski, C. Fryer, D. E. Holz, E. Berti, T. Bulik, I. Mandel, and R. O'Shaughnessy, Astrophys. J. **759**, 52 (2012).

[8] M. C. Miller and D. P. Hamilton, Mon. Not. R. Astron. Soc. **330**, 232 (2002).

[9] T. J. Maccarone, A. Kundu, S. E. Zepf, and K. L. Rhode, Nature (London) **445**, 183 (2007).

[10] S. W. Davis, R. Narayan, Y. Zhu, D. Barret, S. A. Farrell, O. Godet, M. Servillat, and N. A. Webb (LIGO Scientific Collaboration, Virgo Collaboration), Astrophys. J. **734**, 111 (2011).

[11] B. P. Abbott *et al.* (LIGO Scientific Collaboration), Phys. Rev. D **79**, 122001 (2009).

[12] J. Abadie *et al.* (LIGO Scientific Collaboration, Virgo Collaboration), Phys. Rev. D **85**, 082002 (2012).

[13] J. Abadie *et al.* (LIGO Scientific Collaboration, Virgo Collaboration), Phys. Rev. D **83**, 122005 (2011).

[14] J. Aasi *et al.* (LIGO Scientific Collaboration, Virgo Collaboration), Phys. Rev. D **87**, 022002 (2013).

[15] J. Aasi *et al.* (LIGO Scientific Collaboration, Virgo Collaboration), Phys. Rev. D **89**, 102006 (2014).

[16] J. Abadie *et al.* (LIGO Scientific Collaboration, Virgo Collaboration), Phys. Rev. D **85**, 102004 (2012).

[17] J. Aasi *et al.* (LIGO Scientific Collaboration, Virgo Collaboration) (unpublished).

[18] "Advanced LIGO—The next step in gravitational wave astronomy," https://www.advancedligo.mit.edu/.

[19] "Introduction to advanced Virgo," https://wwwcascina.virgo.infn.it/advirgo/.

[20] J. Abadie *et al.* (LIGO Scientific Collaboration, Virgo Collaboration), Classical Quantum Gravity **27**, 173001 (2010).

[21] É. É. Flanagan and S. A. Hughes, Phys. Rev. D **57**, 4535 (1998).

[22] B. P. Abbott *et al.* (LIGO Scientific Collaboration), Phys. Rev. D **80**, 062001 (2009).

[23] B. Allen, Phys. Rev. D **71**, 062001 (2005).

[24] S. Chatterji, L. Blackburn, G. Martin, and E. Katsavounidis, Classical Quantum Gravity **21**, S1809 (2004).

[25] C. A. K. Robinson, B. S. Sathyaprakash, and A. S. Sengupta, Phys. Rev. D **78**, 062002 (2008).

[26] S. Klimenko, I. Yakushin, A. Mercer, and G. Mitselmakher, Classical Quantum Gravity **25**, 114029 (2008).

[27] J. Abadie *et al.* (LIGO Scientific Collaboration, Virgo Collaboration), arXiv:1003.2481.

[28] LIGO Hanford Observatory, http://www.ligo-wa.caltech.edu/.

[29] LIGO Livingston Observatory, http://www.ligo-la.caltech.edu/.

[30] J. Abadie *et al.*, Nucl. Instrum. Methods Phys. Res., Sect. A **624**, 223 (2010).

[31] L. Blackburn *et al.*, Classical Quantum Gravity **25**, 184004 (2008).

[32] J. Abadie *et al.* (LIGO Scientific Collaboration, Virgo Collaboration), Phys. Rev. D **81**, 102001 (2010).

[33] A. Buonanno, Y. Pan, J. Baker, J. Centrella, B. Kelly, S. McWilliams, and J. van Meter, Phys. Rev. D **76**, 104049 (2007).

[34] S. A. Teukolsky, Astrophys. J. **185**, 635 (1973).

[35] J. D. E. Creighton, Phys. Rev. D **60**, 022001 (1999).

[36] E. Berti, V. Cardoso, and C. M. Will, Phys. Rev. D **73**, 064030 (2006).

[37] H. Nakano, H. Takahashi, H. Tagoshi, and M. Sasaki, Phys. Rev. D **68**, 102003 (2003).

[38] D. Talukder, S. Bose, S. Caudill, and P. T. Baker, Phys. Rev. D **88**, 122002 (2013).

[39] J. Abadie *et al.* (LIGO Scientific Collaboration, Virgo Collaboration), Phys. Rev. D **85**, 122007 (2012).

[40] C. Pankow, S. Klimenko, G. Mitselmakher, I. Yakushin, G. Vedovato, M. Drago, R. A. Mercer, and P. Ajith, Classical Quantum Gravity **26**, 204004 (2009).

[41] P. Ajith, M. Hannam, S. Husa, Y. Chen, B. Brügmann, N. Dorband, D. Müller, F. Ohme, D. Pollney, C. Reisswig, L. Santamaría, and J. Seiler, Phys. Rev. Lett. **106**, 241101 (2011).

[42] M. Campanelli, C. O. Lousto, and Y. Zlochower, Phys. Rev. D **74**, 041501 (2006).

[43] L. Rezzolla, P. Diener, E. N. Dorband, D. Pollney, C. Reisswig, E. Schnetter, and J. Seiler, Astrophys. J. Lett. **674**, L29 (2008).

[44] J. Aasi *et al.* (LIGO Scientific Collaboration, Virgo Collaboration), arXiv:1304.0670.

[45] F. Herrmann, I. Hinder, D. Shoemaker, and P. Laguna, Classical Quantum Gravity **24**, S33 (2007).

[46] R. Biswas, P. R. Brady, J. D. E. Creighton, and S. Fairhurst, Classical Quantum Gravity **26**, 175009 (2009).

[47] P. R. Brady and S. Fairhurst, Classical Quantum Gravity **25**, 105002 (2008).

[48] S. Mohapatra, L. Cadonati, S. Caudill, J. Clark, C. Hanna, S. Klimenko, C. Pankow, R. Vaulin, G. Vedovato, and S. Vitale, "Comparing search techniques for studying collisions of binary black holes," https://www.gravity.phy.syr.edu/~satya/Publication-IMR_comparison/ (2014).

[49] J. Aasi *et al.*, Classical Quantum Gravity **31**, 115004 (2014).

[50] LIGO Scientific Collaboration, LSC algorithm library software packages LAL, LALWRAPPER, and LALAPPSL, http://www.lsc-group.phys.uwm.edu/lal.

[51] R. Biswas, P. R. Brady, J. Burguet-Castell, K. Cannon, J. Clayton, A. Dietz, N. Fotopoulos, L. M. Goggin, D. Keppel, C. Pankow, L. R. Price, and R. Vaulin, Phys. Rev. D **85**, 122009 (2012).

[52] P. Ajith *et al.*, Classical Quantum Gravity **29**, 124001 (2012).

[53] A. Taracchini, Y. Pan, A. Buonanno, E. Barausse, M. Boyle, T. Chu, G. Lovelace, H. P. Pfeiffer, and M. A. Scheel, Phys. Rev. D **86**, 024011 (2012).

[54] M. Hannam, P. Schmidt, A. Boh, L. Haegel, S. Husa *et al.*, arXiv:1308.3271.

[55] "Advanced LIGO anticipated sensitivity curves," https://dcc.ligo.org/LIGO-T0900288/public.

[56] G. M. Harry and LIGO Scientific Collaboration, Classical Quantum Gravity **27**, 084006 (2010).

[57] G. Mazzolo *et al.*, "Prospects for intermediate mass black hole binary searches with advanced gravitational-wave detectors," http://arxiv.org/abs/1404.7757.

[58] F. Acernese *et al.* (Virgo Collaboration), "Advanced Virgo Baseline Design," https://tds.ego-gw.it/itf/tds/file.php?callFile=VIR-0027A-09.pdf.

[59] S. Privitera, S. Mohapatra, P. Ajith, K. Cannon, N. Fotopoulos, M. A. Frei, C. Hanna, A. J. Weinstein, and J. T. Whelan, Phys. Rev. D **89**, 024003 (2014).